Article

In Vitro Cytotoxicity and Hemolysis Effect of Poly-Gamma-Glutamic Acid Nano-Polymer Biosynthesized Using Some Isolates of *Bacillus* spp.

Eman M. Elsayed [1,*], Ahmed A. Farghali [2], Mohamed I. Zanaty [3], Medhat Abdel-Fattah [1], Dalal Hussien M. Alkhalifah [4], Wael N. Hozzein [1] and Ahmed M. Mahmoud [1]

[1] Department of Botany and Microbiology, Faculty of Science, Beni-Suef University, Beni-Suef 62521, Egypt; medhat.mahmoud@science.bsu.edu.eg (M.A.-F.); hozzein29@yahoo.com (W.N.H.); ahmed.mahmoud@science.bsu.edu.eg (A.M.M.)

[2] Department of Materials Science and Nanotechnology, Faculty of Postgraduate Studies for Advanced Sciences, Beni-Suef University, Beni-Suef 62521, Egypt; farghali@psas.bsu.edu.eg

[3] Department of Biotechnology and Life Sciences, Faculty of Postgraduate Studies for Advanced Sciences, Beni-Suef University, Beni-Suef 62521, Egypt; zanaty012@psas.bsu.edu.eg

[4] Department of Biology, College of Science, Princess Nourah bint Abdulrahman University, Riyadh 11671, Saudi Arabia; dhalkifah@pnu.edu.sa

[*] Correspondence: emmymicrobiologist@yahoo.com

Abstract: Natural polymers have good biological, biocompatible properties and a low degradation rate, so they can be used in medical applications. This study demonstrates an optimized biosynthesis for poly-gamma-glutamic acid nano-polymer (Ɣ-PGA NP) using three bacterial isolates encoded as B4, B5, and B6. The 16S rRNA gene sequence of the isolates showed 98.5, 99, and 99.8% similarity with *Bacillus* sp., with accession numbers MZ976778, MZ976779, and MZ956153, respectively. The optimal conditions of the biosynthesis were 35 °C, followed by incubation for 30 h, 7 pH, 0.7 $O.D_{600}$ of bacterial broth, carbon sources of glutamic acid and glucose, and ammonium sulfate as the nitrogen source. Biosynthesized Ɣ-PGA NPs were characterized using X-ray diffraction (XRD), Zeta sizer, Fourier transform infrared (FT-IR), transmission electron microscopy (TEM), and nuclear magnetic resonance (^{1}HNMR). The TEM study showed the formation of oval-shaped Ɣ-PGA NPs with sizes 31.75–32.69 nm, 18.63–21.66 nm, and 37.57–39.22 nm for B4, B5, and B6, respectively. XRD, FT-IR, and ^{1}HNMR confirmed the purity of the polymer. The hemolysis rates of the biosynthesized Ɣ-PGA NPs were below the acceptable value. Moreover, the cytotoxicity test conducted using an MTT assay on peripheral blood mononuclear cells (PBMCs) revealed no significant effect on the cell viability within a dose range of up to 512 μg/mL.

Keywords: biosynthesis; biodegradable; Ɣ-PGA; nanopolymer; hemolysis; cytotoxicity

1. Introduction

Broad interest in the possible biodegradation of polymers has developed only in recent years. They can be divided into two categories, synthetic and natural ones. Synthetic polymers can be used in many industrial and medical applications because of their good mechanical properties, as well as their inability to degrade them. One of these applications is orthopedic devices [1]. Natural polymers have good biological, biocompatible properties and a low degradation rate, so they can be used in medical applications. One of these biodegradable polymers is PGA, which is a non-immunogenic homopolymer [2]. PGA is differentiated into two isoforms, (α) and (Ɣ) PGA, depending on the attachment of the carboxy group. α-PGA can be synthesized chemically via the polymerization of the Ɣ-protected N-carboxyanhydride of glutamic acid, while α-PGA cannot be produced microbially [3]. Ɣ-PGA has been synthesized using bacteria, especially genera of the *Bacillus* species [4], and fungi. Bacteria involved in Ɣ-PGA synthesis are mostly Gram-positive bacillus species,

and depending on their need for glutamate, they are classified into glutamate-dependent or non-dependent [5]. ɣ-PGA can either be composed of only D-glutamic acid residues (ɣ-D-PGA), L-glutamic acid residues (ɣ-LPGA), or both of them (ɣ-LD-PGA). ɣ-PGA is different from other proteins because it is polymerized in a ribosome-independent manner inside the cell via ɣ-amide linkages [6,7]. Thus, substances that inhibit the translation of proteins cannot affect its production, and it is also resistant to proteases, which cleave the α-amino linkages [8]. Hence, in this study, the authors decided to use ɣ-PGA as a biomaterial polymer. Furthermore, ɣ-PGA can exist either in a water-insoluble free-acid form or as a salt of a variety of cations, such as Mg^{2+}, Na^+, or K^+, which are completely soluble in water [3,8].

During ɣ-PGA biosynthesis, L-glutamic acid units that makeup ɣ-PGA can be derived via the glutamic acid biosynthetic pathway. L-glutamic acid units can be obtained either exogenously or endogenously [9].

L-glutamic acid endogenously is produced by converting a carbon source via acetyl-CoA and TCA cycle intermediates. Then, α-Ketoglutaric acid from the TCA cycle is used as the direct precursor of glutamic acid synthesis [9]. In the case of exogenous, L-glutamic acid can be converted into L-glutamine by the enzyme glutamine synthase. In addition, L-glutamine is a precursor of ɣ-PGA. ɣ-PGA biosynthesis needs the pgsBCA genes that lie on large plasmids or chromosomes [10,11]. Capsule (cap) genes and pgs (polyglutamate synthase) genes are required to release ɣ-PGA when it is associated with a capsule (as in *Bacillus anthracis*) [8].

The Mw of ɣ-PGA can vary according to many factors, such as the used strain of bacteria or fungi, the chemical components of the media, and the physical conditions. Some studies have produced high and low Mw of ɣ-PGA, ranging up to 2000 kDa, which could be applied in many fields according to the Mw value, such as in food and water applications [12], and in the bioengineering field. ɣ-PGA with a high Mw is preferable for applications such as the construction of scaffolds and hydrogels [13–15], while low-Mw ɣ-PGA is desirable for drug delivery applications, thus allowing for the diffusion of the molecules [14–19]. Moreover, the ɣ-form of PGA has been used in several applications in the biomedical field [3], either in the development of nanosystems for the controlled release of drugs; tissue regeneration; biodegradable fibers; hydrogels; biological adhesives; thickeners; humectants; and a broad range of industrial fields, such as cosmetics, water treatment, and food [11].

Nanotechnology has been applied in the medical field for drug delivery, disease treatment, enhancing treatments, etc. This is because nanoparticles have unique physical and biological properties because of their characteristic sizes, which affect their properties [16]. Nanoparticles have many additives in polymeric matrices, with the goal of improving not only their bioactivity but also their mechanical strength, hydrophilicity, and tissue-attracting strength. Moreover, small-size nanoparticles have been found to be more efficient as antimicrobials and anti-tumor agents because they can pass through cell walls [17]. Knowledge of the interactions between human cells and nanoparticles has great importance for the design of non-toxic medical applications [18].

Peripheral blood mononuclear cells (PBMCs) include lymphocytes (T cells, B cells, and NK cells), monocytes, and dendritic cells. Recent works have studied the various in vitro cytotoxicity values of nanoparticles with respect to cell type and size. Cell-mediated immunity includes different cells. These cells include T cells (i.e., CD^{8+}, CD^{4+}, and ɣ/δ T cells) and T cell-derived cytokines that play an important role in the defense against microbial infections. It was found that T cells have the ability to proliferate in response to each antigen. Among the existing cytokines, IFN-ɣ is a key cytokine in the control of bacterial infections. It is secreted by T cells and Natural Killer (NK) cells, which play an important role in the activation of macrophages, which kill intracellular bacterial infections [19]. Moreover, Mast cells participate in inflammation and allergies by secreting many pro-inflammatory mediators [20]. Furthermore, monocytes are important in anti-inflammatory and inflammatory processes.

In the present study, we used PBMCs in the cytotoxicity test in order to study ɤ-PGA NPs' effect on the immune system.

Previous studies focused on changing parameters to get more ɤ-PGA yield to be used for the applications mentioned above. No paper studied getting small-sized ɤ-PGA NP to be used as a biopolymer agent. For example, Xu et al., 2019 focused on the ɤ-PGA yield produced using a metabolically engineered *Corynebacterium glutamicum* ATCC 13032, carrying capBCA. They found that *C. glutamicum* ATCC 13032 produced ɤ-PGA up to 11.4 g/L, showing a higher titer compared with *C. glutamicum* F343 expressing pgsBCA [21]. Wei et al., 2014 studied the effects of multiple physicochemical stresses on the production and synthetase genes transcription of ɤ-PGA using *Bacillus licheniformis* WX-02. They showed that the maximum ɤ-PGA yield reached 29.34 g L^{-1} [22]. Also, Qiu et al., 2019 found that *Bacillus amyloliquefaciens* NX-2S154 was obtained through atmospheric and room temperature plasma mutagenesis, which produced 14.83 ± 0.31 g/L of ɤ-PGA [23]. In the present work, we studied the effect of many factors to produce nano-sized ɤ-PGA. As mentioned in previous works, small-sized nanoparticles are more effective in many medical applications, such as using them as antimicrobial agents [24].

Interestingly, there were studies about the cytotoxicity of ɤ-PGA-based nanoparticles. As concluded by Pisani et al., 2019, ɤ-PGA/chitosan showed an initial 80% cell viability on human dermal fibroblasts. Therefore, we surmised that biosynthesizing a biodegradable NP may be non-toxic for normal cells and highly effective for biomedical applications [25]. Therefore, we surmised that biosynthesizing a biodegradable NP may be non-toxic for normal cells and highly effective for biomedical applications. We also aimed to biosynthesize NP with negligible cytotoxicity, because some metal nanoparticles showed cell viability around 90% as shown by Lv et al., 2021 who tested Ag nanoparticles against L929 fibroblast cells [26].

Consequently, in this study, biodegradable ɤ-PGA NPs were biosynthesized in small sizes, which were not previously obtained. Different concentrations of NPs were tested for their safety towards blood hemolysis and PBMCs were used for further medical applications.

2. Materials and Methods

2.1. Isolation and Screening of Bacillus Isolates for the Ability to Synthesize ɤ-PGA NPs

For bacterial isolation, samples were prepared by adding 10 gm of each sample into 100 mL saline solution. Those samples were dried manure, skim milk, and dried poultry manure. Then, suspensions were incubated with shaking for 30 min, and 0.1 mL of each sample was inoculated for bacterial isolation using an NA medium. Pour, surface, and soil plate methods were performed with incubation at 30, 35, and 40 °C, and a Gram stain was carried out to confirm the isolates [27].

For ɤ-PGA NPs biosynthesis, each bacterial isolate was allowed to grow aerobically for 24 h at 37 °C in 100 mL of a medium containing 1 g polypeptone, 0.2 g yeast extract, and 0.1 g MgSO$_4$.7H$_2$O. Biosynthesis of ɤ-PGA NPs was maintained by annealing bacterial cells for 10 min at 60 °C to form spores. The spore suspension (0.5 mL) was inoculated into 100 mL of the sterilized medium, adjusted to pH 7.5, in 500 mL flasks containing 1 g of L-glutamic acid, 2 g glucose, 0.5 g ammonium sulfate, 0.1 g KH$_2$PO$_4$, 0.1 g Na$_2$HPO$_4$.12H$_2$O, 0.05 g MgSO$_4$.7H$_2$O, 0.002 g MnSO$_4$.nH$_2$O, 0.005 g FeCl$_3$.6H$_2$O, 0.02 g CaCl$_2$, and 50 μg biotin (vitamin H). Cultivation was performed aerobically with shaking (120 rpm) at 37 °C [12].

2.2. Isolation and Purification of ɤ-PGA NPs

This was performed according to Goto and Kunioka, 2005 [28], with some modifications as follows.

First, the fermented liquid was centrifuged at 12,000× g for 5 min at 4 °C. Then, the pH of the supernatant was adjusted to 3.0 with H$_2$SO$_4$ (6 M) and incubated for 12 h at 4 °C. Then, the solution was filtered, diluted with three folds of 70% ethanol, and left for half an hour for precipitation. Afterward, centrifugation was performed for 5 min at 20,000 rpm

at room temperature and the precipitate was dissolved in 0.2 M HCl, then the pH of the media was adjusted to 8.0 using 0.1 M NaOH. The solution containing ɤ-PGA NPs was then purified through dialysis three times against distilled water at 25 °C [12].

2.3. Characterization of the Biosynthesized ɤ-PGA NPs

Visual observation of the change of culture filtrate viscosity indicates the formation of ɤ-PGA NPs concomitant to bacterial growth [29]. To determine the average size of the biosynthesized ɤ-PGA NPs, laser diffractometry, using Zeta sizer nano-series (Nano ZS) Malvern Instruments, Malvern, UK was used. Measurements were taken in the range between 0.6:6000 nm. Isolates that synthesized the smallest NPs were further identified by PCR technique.

2.4. 16S rRNA Gene Sequencing for the Molecular Identification of the Selected Isolates

The molecular identification of the selected isolates was determined based on sequencing of the 16S rDNA gene at the Sigma lab.

Total genomic DNA was extracted, using GeneJet genomic DNA purification Kit (Thermo), for PCR [30]. The bacterial precipitate of 2 mL nutrient broth culture was resuspended in 180 µL of digestive solution 20 µL of Proteinase K Solution was added, then the sample was incubated at 56 °C while vortexing. After that, 20 µL of RNase A Solution was mixed and the mixture was incubated for 10 min at 37 °C. The solution was lysed using 200 µL of Lysis by vortexing for about 15 s. Then, 50% ethanol (400 µL) was added. After that, the prepared lysate was transferred to a GeneJET™ Genomic DNA purification column and inserted in a collection tube, which was centrifuged for 1 min. The extracted DNA was then used as a template for PCR with the primers F: 5′- AGA GTT TGA TCC TGG CTC AG-3′ and R: 5′- GGT TAC CTT GTT ACG ACT T-3′. The total volume of the PCR reaction was 50 µL. PCR amplifications were performed with the temperature profile cycles described by Prasad and Turner, 2011 [31]. After that, PCR reaction products were analyzed by agarose gel electrophoresis. The product was then purified, subjected to sequencing PCR using the GeneJET™ purification column, and sequenced at GATC Company with ABI 3730xl DNA sequencer (Germany). Afterward, DNA sequences were used for BLAST and phylogenetic analysis [32].

2.5. Optimization of the Biosynthesized ɤ-PGA NPs

Five parameters related to the studied medium, namely temperature (30, 35, 40, and 50 °C), incubation time (12, 24, 30, 36, 48, and 72 h), pH (6, 7, 8, 9, and 10), carbon and nitrogen sources (Table 1), and bacterial O.D$_{600}$ (0.5, 0.7, and 1), were adjusted to optimize the biosynthesis of the ɤ-PGA NPs.

Table 1. Different carbon and nitrogen sources into the media to produce ɤ-PGA NPs.

1st C and N Source	2nd C and N Source	3rd C and N Source	4th C and N Source
Glutamic acid	Glucose	Citric acid	Glutamic acid
Glucose	Ammonium Sulfate	Ammonium Sulfate	Glucose
Ammonium sulfate	KH$_2$PO$_4$	KH$_2$PO$_4$	KH$_2$PO$_4$
KH$_2$PO$_4$	Na$_2$HPO$_4$.12H$_2$O	Na$_2$HPO$_4$.12H$_2$O	Na$_2$HPO$_4$.12H$_2$O
Na$_2$HPO$_4$.12H$_2$O	MgSO$_4$.7H$_2$O	MgSO$_4$.7H$_2$O	MgSO$_4$.7H$_2$O
MgSO$_4$.7H$_2$O	MnSO$_4$.nH$_2$O	MnSO$_4$.nH$_2$O	MnSO$_4$.nH$_2$O
MnSO$_4$.nH$_2$O	FeCl$_3$.6H$_2$O	FeCl$_3$.6H$_2$O	FeCl$_3$.6H$_2$O
FeCl$_3$.6H$_2$O	CaCl$_2$	CaCl$_2$	CaCl$_2$
CaCl$_2$			Biotin
Biotin			

2.6. Characterization of the Optimized Biosynthesized ɤ-PGA NPs

XRD experiments were performed on a PANalytical (Empyrean) X-ray diffraction (analytical-x' pertpro, Cukα1 radiation, λ = 1.5404 Å, 45 kV, 40 mA, The Netherlands)

by Cu-Kα radiation operating with a CuKα2 (λ = 0.154060 nm). The applied current and the accelerating voltage were 30 mA and 40 kV, respectively, as described by Chen et al., 2018 [33]. Bruker spectrometer was utilized to record FT-Raman spectra (Thermo Fisher Scientific Inc., Pittsburgh, PA, USA) before and after the adsorption of Cd^{+2} metal ions [33]. The wavenumber range of 4000–400 cm^{-1}, with a resolution of 0.5 cm^{-1}. An automated routine co-added 7200 interferograms collected at the given resolution and the resultant interferograms were Fourier transformed. TEM images were taken, with 200 kV acceleration voltage, by JEOL-JEM 2100 (Japan). ^{1}H NMR DEPT-Q (Switzerland) was performed using the Bruker instrument at 400 MHz after dissolving the sample into heavy water (D_2O) [34].

2.7. In Vitro Hemolysis Assay

This study was approved by the institutional review board of Beni-Suef University, Egypt (BNS/2021/10). All experiments were performed in accordance with Beni-Suef University guidelines. Informed consent was obtained from all the participants.

The hemolysis assay was conducted as stated by Khan et al., 2015 [35], with some modifications. To separate serum and collect fresh red blood cells (RBCs), a total of 2 mL of blood containing 1 mL EDTA was immediately centrifuged at 2500 rpm at 4 °C for 5 min. RBCs were washed 3 times and diluted with PBS to reach a 4% hematocrit. Then, 50 μL was taken to 50 μL of each of the utilized nanopolymer concentrations (1, 2, 4, 8, 16, 32, 64, 128, 256, and 512 μg/mL), deionized water and PBS served as positive and negative control, respectively. All preparations were conducted in triplicates and incubated for 8, 12, 24, and 48 h, at 37 °C. After that, the ELISA (Tecan Group Ltd., Mannedorf, Switzerland) test was used to assess the absorption of hemoglobin in the supernatant at 570 nm [36]. Hemolysis percent was calculated as percent hemolysis (%) = [(sample absorbance − negative control)/(positive control − negative control)] × 100% [37].

2.8. In Vitro Cytotoxicity

2.8.1. Toxicity Tests in PBMCs

To investigate the immune response to ɣ-PGA NPs, mononuclear cells (monocytes and lymphocytes) were separated with a glycerol density gradient, according to Aimola et al., 2013 [38]. Blood samples (2 mL) were collected in tubes with EDTA and then diluted two times with PBS (pH 7.2). Afterward, blood (1 mL) was combined with 1 mL of glycerol gradient (1.077 g/mL). The glycerol gradient was carried out by adding 1.68 mL into 25 mL of sterile water. NaCl (1.2) was added, making up 10% of the total volume [38]. The integrity of the isolated cells necessitates a gradient isotonic with the intracellular environment which in turn is necessary for the cell isolations [39]. Samples were then centrifuged for 30 min at 2500 rpm. The buffy coat layer, with mononuclear cells, was warily assembled in sterile conditions using a disinfected pipette and then moved to sterile tubes. PBS was used to wash cells three times, then cells were cultured on RPMI 1640 medium augmented with L-glutamine for 24–72 h at 37 °C in a humidified atmosphere of 5% CO_2, in order to stimulate cells proliferation.

2.8.2. Cytotoxicity by MTT Assay

After incubation with RPMI, 10^6 cells/well were transferred into 96-well culture plates with the tested concentrations of ɣ-PGA NPs and incubated for 24 h at 37 °C. Next, cells were incubated with 20 μL of MTT for 4 h at 37 °C. Finally, DMSO (50 μL) was added for the solubilization of the formed formazan crystals. The experiment was conducted in triplicate. After that, an ELISA reader (Tecan Group Ltd., Mannedorf, Switzerland) was used to determine the absorbance at 550 nm. Human PBMCs treated with PBS served as negative controls [36].

2.9. Statistical Analysis

One-way analysis of variance (ANOVA) was used for statistical analysis of in vitro results. The $p < 0.05$ was ascribed as statistically significant. The one-way analysis of variance was used to determine statistical differences between groups (SPSS version 20 software, Chicago, IL, USA). All the biological quantitative data are presented as mean $\pm$ standard deviations (SD).

3. Results and Discussion

3.1. Ability of Bacillus spp. Isolates to Biosynthesis ɣ-PGA NPs

Bacilli have been indicated for their ability to synthesize ɣ-PGA. Here, seven isolates were tested for producing ɣ-PGA. Primary identification using Gram stain was allowed to obtain this test. Of note, the viscosity of the isolates' filtrate was increased, which is indicative of the biosynthesis of ɣ-PGA. Sizes of ɣ-PGA NPs biosynthesized from each isolate were recorded in (Table 2) and (Figure 1). It is clear that isolates encoded B4, B5, and B6 could synthesize the smallest NP sizes.

**Table 2.** Particle size of ɣ-PGA NPs synthesized by *Bacillus* spp. isolates.

Microbial Isolates	ɣ-PGA NPs Size (nm)
B1	340
B2	342
B3	615
B4	218
B5	190
B6	220
B7	615
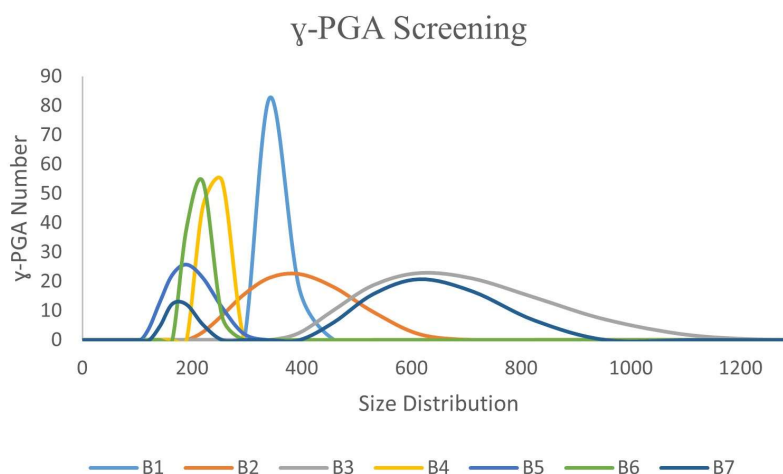
Figure 1. Relation between size distribution of ɣ-PGA NPs and screened bacterial isolates.

3.2. Molecular Identification and 16S rDNA Sequence-Based Phylogenetic Analysis of the Isolates

The USA database of the National Center for Biotechnology Information (NCBI), using the Basic Local Alignment Search Tool for Nucleotides (BLASTN), was performed to align the sequences of 16S rDNA gene of the isolates and compare them with those in the GenBank, and a phylogenetic tree was drawn using Mega (version 7) as shown in (Figure 2).
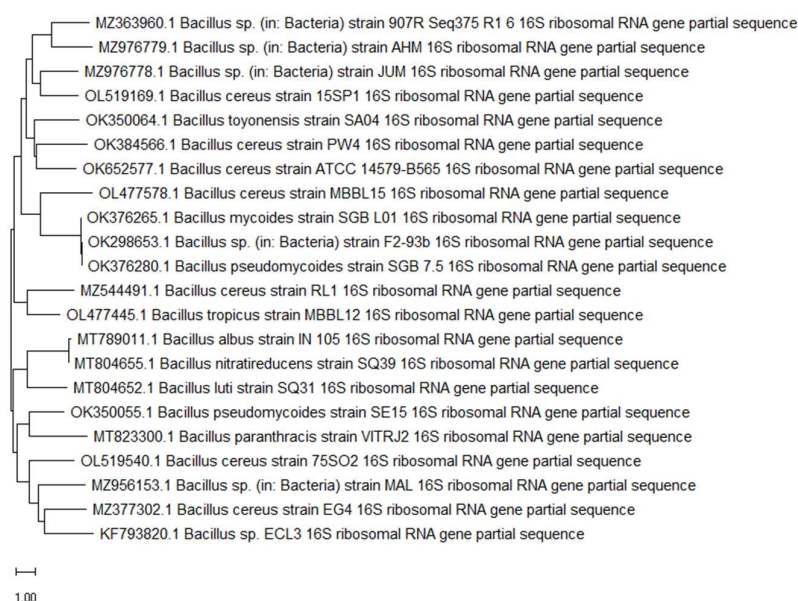
Figure 2. Phylogenetic analysis of 16S rRNA sequences of the isolates B4, B5, and B6.

The sizes of the 16S rRNA ribosomal PCR amplified products were 917, 492, and 498 bp for B4, B5, and B6, respectively. The 16S rRNA gene sequences showed 98.5, 99, and 99.8% similarity with *Bacillus* spp. in the GenBank database [40].

Bacterial isolates encoded B4, B5, and B6 have accession numbers of MZ976779, MZ976778, and MZ956153, respectively. They were proposed to be named *Bacillus benisuefensis* sp. nov., *Bacillus nileeastensis* sp. nov., and *Bacillus naeemensis* sp. nov., for B4, B5, and B6, respectively.

3.3. Optimization of the Conditions of ɤ-PGA NPs Biosynthesis

In the current study, several methods were used to biosynthesize small ɤ-PGA NPs. Conditions that gave the smallest size of ɤ-PGA NPs for the three bacterial strains were (35 °C, 30 h of incubation, 7 pH, group no. 1 of C&N sources, and 1 O.D$_{600}$ of the bacterial growth).

The smallest size was synthesized using glutamic acid and glucose as carbon sources, ammonium sulfate as nitrogen source, and bacterial O.D was 0.7. In this study, the particle size decreased with increasing temperature up to 35 °C, incubation time up to 30 h, and pH up to 7. After that, ɤ-PGA particle size increased. A remarkable increase in the particle size of the biosynthesized ɤ-PGA NPs was observed with citric acid as a carbon source and glutamic acid as a nitrogen source. It is notable that previous papers studied changed the chemical composition of the microbial media to increase the ɤ-PGA yield. This was shown by Shih and Van (2001) [11] who succussed in order to increase the ɤ-PGA yield by using 20 g/L L-glutamic acid, 12 g/L citric acid, 80 g/L glycerol, 7.0 g/L NH$_4$Cl, 0.5 g/L MgSO$_4$, 0.04 g/L FeCl$_3$.6H$_2$O, 0.5 g/L K$_2$HO$_4$, and pH 7.4 with NaOH, and incubating for 3–4 days that allowed ɤ-PGA production of 15 g/l by using *B. licheniformis* ATCC9945A.

Previous papers did not study the effect of chemical, physical, or biological conditions on ɤ-PGA size but they studied the effect of some parameters on ɤ-PGA yield. In that context, Ko and Gross, 1998 [9] proved that ɤ-PGA produced with low yield at high pH, while they found that ɤ-PGA yield increased from 22 to 48 h. In the same context, Shih and Van, 2001 [11] concluded that ɤ-PGA yield was highest at pH 6.5 and 96 h.

3.4. X-ray Diffraction and Microstructure Analysis of ɤ-PGA NPs

The XRD pattern of ɤ-PGA NPs synthesized by the three strains demonstrated that it exists in the salt form (Figure 3), which proves the first result of the produced soluble solution, as mentioned before by Ogunleye et al., 2015 [4]. The main peaks of potassium

poly gamma glutamate appeared at 21, 25, and 31°θ and a broad peak between 20 and 30°θ. The broad peak between 21 and 32°θ proves ɣ-PGA presence. Moreover, wide peaks, which prove the amorphous phase of the specimen, observed at these angles appeared due to the polymer chains of ɣ-PGA [41]. Another study by Panda et al., 2021 [42] found that the pure PGA showed a semi-crystalline diffraction peak of 2θ value at around 22.68°.
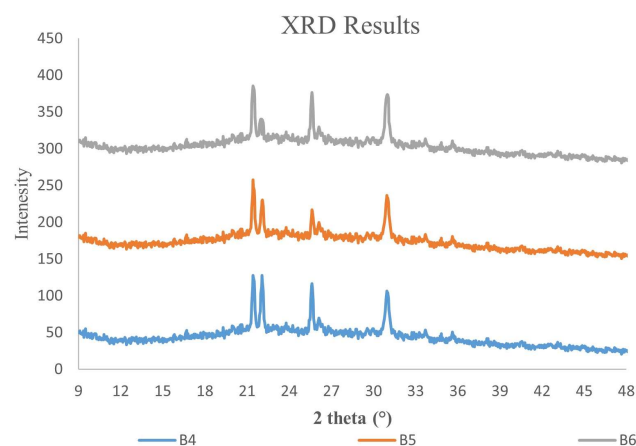
Figure 3. XRD peaks of ɣ-PGA NPs synthesized from the *Bacillus* strains.

Compared with previous work, this broad peak is consistent with that reported by Lee et al., 2011 [43], who showed that ɣ-PGA was produced into the medium with broad peaks at 21 and 31°θ. Also, Chen et al., 2018 [33] demonstrated the broad peak of ɣ-PGA between 20 and 30°θ.

Also, sharp peaks at 21, 25, and 31°θ prove the crystalline nature of K$^+$ as indicated by Liu et al., 2018 [44]. So, these peaks prove the presence of potassium poly-gamma-glutamate. On the other hand, crystalline peaks doped inside the hump one may prove the poly-crystalline nature of the potassium poly-gamma-glutamic acid.

3.5. FT-IR of ɣ-PGA NPs

FTIR analysis was studied to confirm the biosynthesis of ɣ-PGA NPs by the selected isolates, showing the similarity of such figures indicating the biosynthesis of ɣ-PGA NPs; however, these figures have some observed changes and shifts in transmission spectra in the range of 500–4000 cm^{-1}, as presented in (Figure 4a–c). The FTIR bands approximately between 900 and 650 cm^{-1} presented the amid groups of ɣ-PGA [45]. Preparation of ɣ-PGA NPs behavior in salt solutions with different ionic valence numbers. The slight shift of the bands of ɣ-PGA indicated the influence of bacterial isolates in the biosynthesis of ɣ-PGA NPs. This shift, at band 2365 cm^{-1} in (Figure 4b,c) which was at 2111 cm^{-1} in (Figure 4a), may be due to the presence of slight traces of polysaccharides.

As shown in Figure 4, a characteristic band for the carboxylic acid salt appeared at 1597 cm^{-1}. Also, the distinctive absorption of the C=O in secondary amides (amide I band) appeared overlapping the characteristic band for –COO$^-$. Additionally, the typical vibration bands of ɣ-PGA NPs were also revealed in FT-IR analysis at wavelengths 1567, 1123, and 616 cm^{-1} with high intensity. As appeared in FT-IR analysis, absorption for potassium ɣ-polyglutamate in KBr pellets was as follows: Amide I, bending N-H band at 1567 cm^{-1}, Amide II, inconspicuous stretching band because of the strong ionic complexation, symmetric C=O stretching band at 1412 cm^{-1}, stretching C-N band at 1123 cm^{-1}, bending N-H band at 616 cm^{-1}. Also, the transmission band at 3449 cm^{-1} is a characteristic of the O-H stretching vibration of the hydroxyls in the carboxyl groups with high intensity. Similarly, Chen et al., 2018 [33] observed FT-IR bands at 3427 cm^{-1} and 2973 cm^{-1} because of the stretching vibrations of O-H and N-H and -CH and -CH2, respectively. These results also agree with bands observed by Ogunleye et al., 2015 [4]. In the same

context, Panda et al., 2021 [42] presented that the FT-IR bands of ɤ-PGA resemble the bands observed in this study.

FT-IR

(**a**)

FT-IR

(**b**)

FT-IR

(**c**)
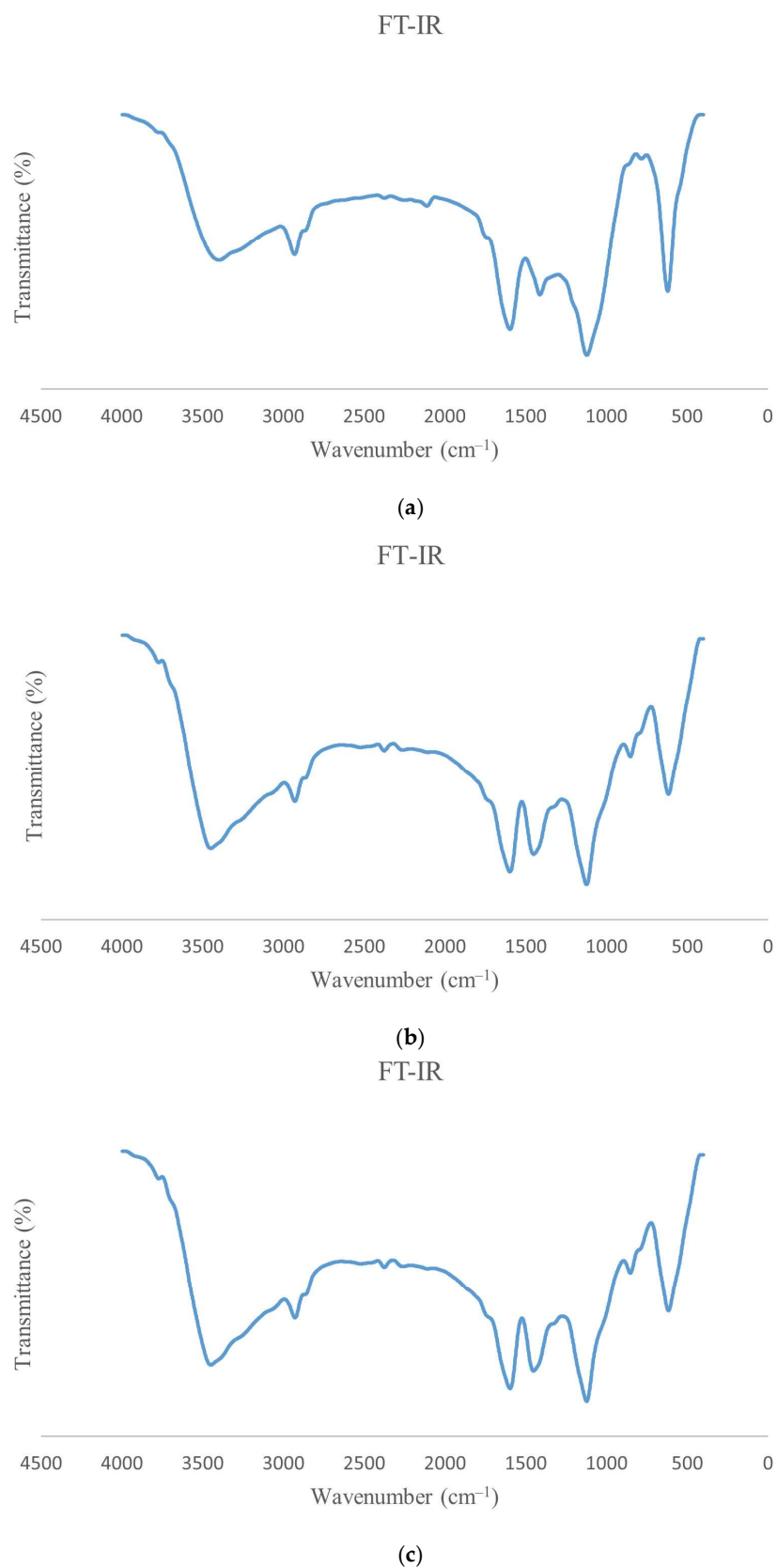
Figure 4. (**a**–**c**) FT-IR spectra of ɤ-PGA NPs synthesized by B4, B5, and B6, respectively.

Figure 4b,c showed more similarity at 848 cm^{-1}, 1545 cm^{-1}, and 2372 cm^{-1}, which slightly differ from that presented in Figure 4a. These results might be correlated to the bacterial isolates polysaccharides that are produced during the ɣ-PGA NPs biosynthesis. Interestingly, the polysaccharides present in the specimens were of few amounts because of the absence of extra bands of other function groups.

The area under bands at the three IR data (Figure 4) shows the similarity between them in the purity of biosynthesized ɣ-PGA NPs. The FTIR data confirmed the biosynthesis of ɣ-PGA NPs by the *Bacillus* spp.

3.6. TEM Imaging

The TEM micrographs (Figure 5a–c) show the morphology and size of ɣ-PGA NPs. The ɣ-PGA NP particles are in an oval shape with a size of ɣ-PGA NPs 31.75–32.69 nm, 18.63–21.66 nm, and 37.57–39.22 nm for B4, B5, and B6, respectively. No previous works imaged the shape or size of ɣ-PGA NPs, while some previous studies used ɣ-PGA as a drug carrier for the desired nanoparticle and measured their total size. A previous study by Pereira et al. (2012) [46] showed that Ch/ɣ-PGA nanocomplexes were almost spherical in shape with a size of 100–200 nm. Hajdu et al. (2008) [47] imaged Ch/ɣ-PGA using TEM, which showed them as spherical with 500 nm. Also, TEM images of Nguyen et al., 2019 [48] for ɣ-PGA/Alum showed a particle size of 1294.67 ± 13.32 nm.


(a)   (b)

(c)
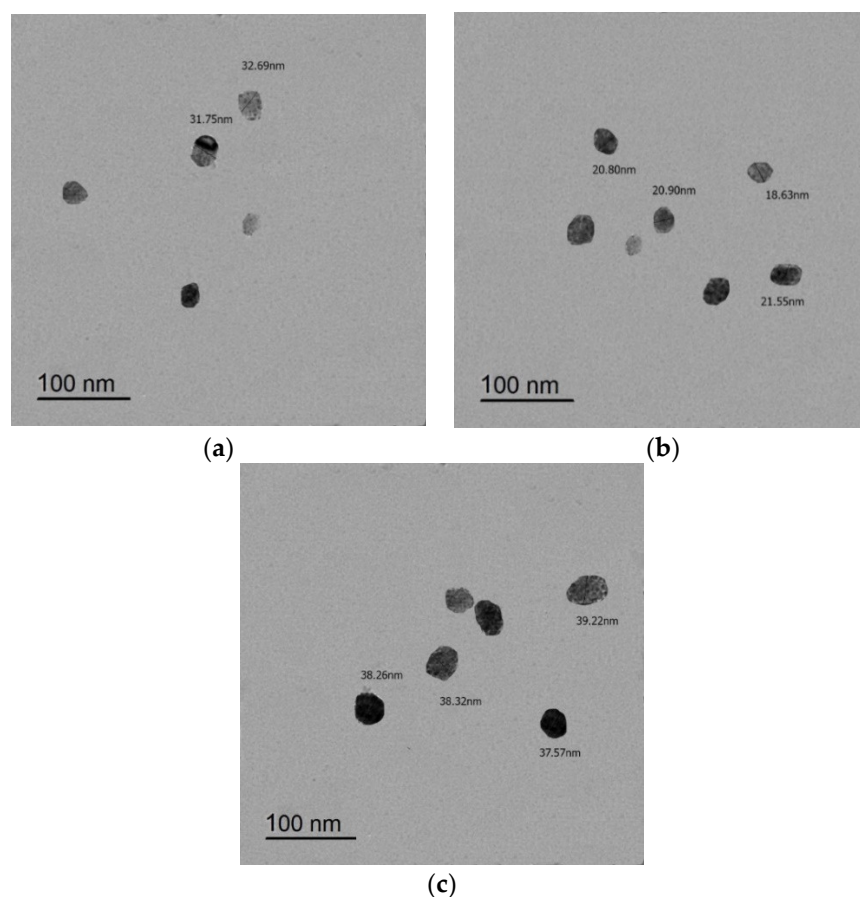
Figure 5. (**a**–**c**) TEM images of oval ɣ-PGA NPs biosynthesized by B4, B5, and B6, respectively.

3.7. NMR Results

^{1}H NMR spectrum complements FT-IR analysis of ɣ-PGA NPs. As shown in Figure 6, the chemical shift in ppm at 1.96–2.2, 2.24, 3.55–3.80, and 8.37 ppm represents protons of β-CH2, ɣ-CH2, α-CH2, and amide, respectively. So, they are consistent with the positions of the peaks of the standard ɣ-PGA NPs. These data are compatible with those of Akagi et al., 2007 [6]. Thus, ^{1}H NMR and FT-IR spectra coincided with the expected spectra for

ɤ-PGA NPs. Furthermore, the high quality and purity of the biosynthesized ɤ-PGA NPs were inferred from the almost absence of additional unexpected signals in the spectra, which ensures the data of FT-IR. Similarly, Anju et al., 2017 [49] showed the peaks of ɤ-PGA at ppm 1.95–2.07 ppm (β, 2H), 2.26–2.28 ppm (ɤ, 2H), and 3.66–3.69 (α,1H). On the other hand, Khalil et al., 2016 [34] indicated impurity peaks at ^{1}H NMR result of ɤ-PGA which is produced by *B. subtilis*.
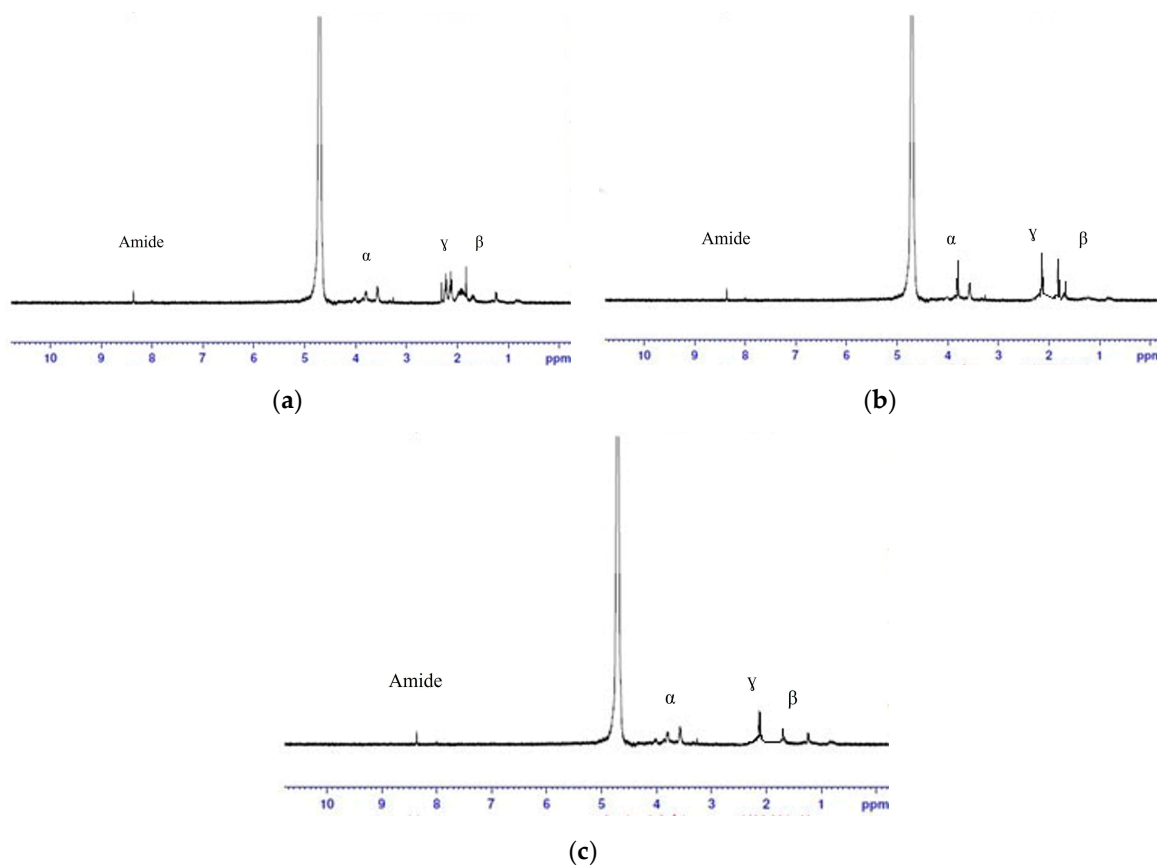

Figure 6. (**a**–**c**) ^{1}H-NMR spectrum of ɤ-PGA NPs synthesized by B4, B5, and B6, respectively. The peak of 4.7 ppm corresponds to the D_2O used as a solvent.

3.8. Hemolysis Assay

To evaluate the biocompatibility of the nanocomposites, hemolysis rates of ɤ-PGA NPs were detected. They were acceptable (Figure 7) since negligible hemolysis was detected. Those data were acceptable even at high concentrations of ɤ-PGA NPs (528 μg/mL), which was less than 4 % (* $p < 0.05$), as shown in (Table 3). 3.9 That may be because ɤ-PGA NPs' different concentrations did not stimulate osmotic hemolysis of the whole blood [50]. Also, there was a slight van der Waals force between the ɤ-PGA NPs and the blood, as well as there was negligible interaction between them and red blood corpuscles [51]. Thus, the ɤ-PGA NPs could be exploited in applications incorporating blood contact.

Some previous works studied the effect of other nanoparticles or nanocomposites against blood. One of those works was allowed by Lu et al., 2018 [52], who proved that the Ch-Au@MMT nanocomposites yielded hemolysis rates below the acceptable value of 10%, even when the nanocomposite concentration was as high as 128 μM (much higher than their respective MIC), while Khan et al., 2015 [26] found that TiO_2 and ZnO nanoparticles showed 52.5% and 65.2% hemolysis, respectively, at 250 ppm.
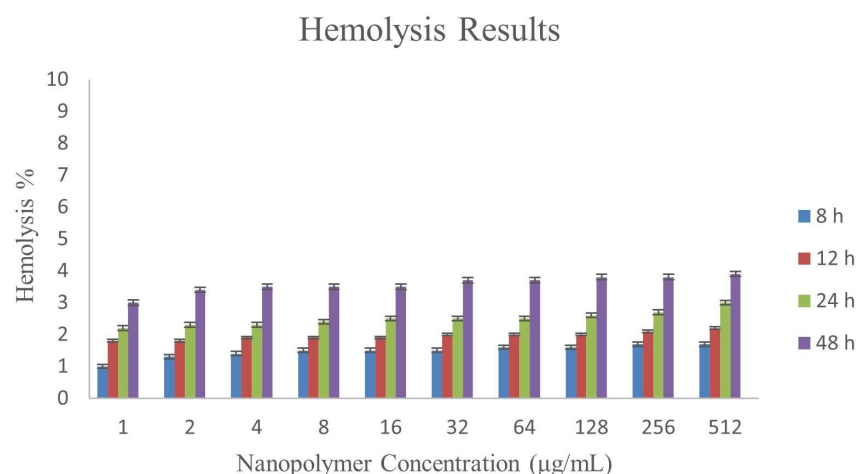
Figure 7. Hemolysis in human erythrocytes treated with ɤ-PGA NPs.

Table 3. Hemolysis effect of ɤ-PGA NPs.

ɤ-PGA NPs Concentration (µg/mL)	Hemolysis %			
	8 h	12 h	24 h	48 h
1	1 ± 0.024	1.8 ± 0.031	2.2 ± 0.023	3 ± 0.047
2	1.3 ± 0.028	1.8 ± 0.036	2.3 ± 0.026	3.4 ± 0.04
4	1.4 ± 0.035	1.9 ± 0.019	2.3 ± 0.021	3.5 ± 0.042
8	1.5 ± 0.032	1.9 ± 0.025	2.4 ± 0.014	3.5 ± 0.041
16	1.5 ± 0.031	1.9 ± 0.042	2.5 ± 0.019	3.5 ± 0.032
32	1.5 ± 0.03	2.0 ± 0.012	2.5 ± 0.023	3.7 ± 0.029
64	1.6 ± 0.022	2.0 ± 0.043	2.5 ± 0.027	3.7 ± 0.04
128	1.6 ± 0.022	2.0 ± 0.04	2.6 ± 0.037	3.8 ± 0.019
256	1.7 ± 0.024	2.1 ± 0.035	2.7 ± 0.038	3.8 ± 0.034
512	1.7 ± 0.025	2.2 ± 0.035	3 ± 0.039	3.9 ± 0.02

Data are expressed as mean $\pm$ S.D.

3.9. Impact of the ɤ-PGA NPs on Cell Viability in PBMC

After the treatment of proliferative blood cells with the different concentrations of ɤ-PGA NPs for 24 h, cell viability was investigated using an MTT assay. No remarkable changes in the PBM cell number were observed (Figure 8). Up to 512 µg/mL, ɤ-PGA NPs maintained high cell viability over 90% (* $p < 0.05$), as shown in (Table 4). This proves the safety of ɤ-PGA NPs on the immune system.

The physical properties of NPs such as surface and size determine their biological impact. NP shapes such as spherical, and rod shapes showed unselective cytotoxicity and spherical-shaped NPs decrease cell viability in human cells, as proved by Reddy et al. 2007 [53].

Previous studies have determined that toxicity occurs in a cell-dependent manner. So, as discussed by Hanley et al., bacterial cells are killed at lower NP concentrations than human T cells [54]. Knowing that PBMC consists of NK cells and lymphocytes (B cells and T cells), PBMC consists of about 45–70% T cells. Also, the outside environment of human cells is a positive charge that determines the NPs' cytotoxic selectivity. Hence, normal human cells cannot attract positively charged ɤ-PGA NPs.

Nguyen et al., 2019 [48] showed that ɤ-PGA/Alum has no cytotoxicity effect on bone marrow-derived cell lines.

Cytotoxicity Assay
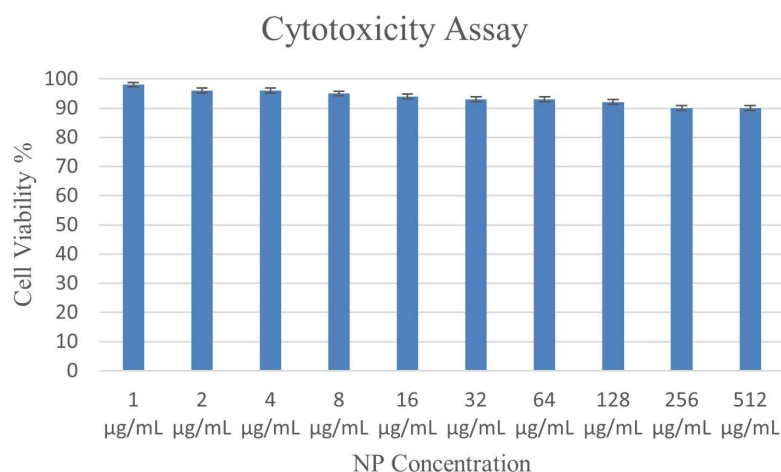
Figure 8. Cell viability test by MTT assay in PBMCs treated with different concentrations of ɤ-PGA NPs for 24 h.

Table 4. The effect of ɤ-PGA NPs on PBMCs at different concentrations.

ɤ-PGA NPs Concentration (µg/mL)	Percentage of Treated Cells
1	98 ± 0.68
2	96 ± 0.2
4	96 ± 0.48
8	95 ± 0.57
16	94 ± 0.29
32	93 ± 0.63
64	93 ± 0.21
128	92 ± 0.3
256	90 ± 0.73
512	90 ± 0.4

Data are expressed as mean ± S.D.

On the other hand, some papers focused on uploading drugs on ɤ-PGA, as indicated by Tsai et al., 2014 [55], who tested the effect of ɤ-PGA/doxorubicin (DXR) on hepatoma cells. They noticed that the cell viability for 500 ng/mL ɤ-PGA/DXR was 66.5%, due to the increased uptake of DXR.

4. Conclusions

In the present study, *Bacillus* spp. isolates were isolated using different sources. Those isolates were used to biosynthesize ɤ-PGA NPs. ɤ-PGA NPs were purified, and their sizes were measured using a Zeta sizer instrument. After detecting that B4, B5, and B6 produced the smallest ɤ-PGA NPs size, they were identified using 16S rRNA, and different chemical, physical, and biological conditions were adjusted to B4, B5, and B6 to optimize the biosynthesis of the ɤ-PGA NPs.

The 16S rRNA gene sequences showed 98.5, 97, and 99% similarity with *Bacillus* spp. in the GenBank database. After that, the three bacterial isolates had accession numbers of MZ976778, MZ976779, and MZ956153, respectively. They were proposed to be named *Bacillus benisuefensis* sp. nov., *Bacillus nileeastensis* sp. nov., and *Bacillus naeemensis* sp. nov., for B4, B5, and B6, respectively.

Then, the purified ɤ-PGA NPs have been characterized by XRD, TEM, FT-IR, and ^{1}HNMR. XRD peaks at 21, 25, and 31°θ proved the presence of potassium poly gamma glutamate, and the broad peak between 20 and 30°θ proved ɤ-PGA presence. Moreover, wide

peaks, prove the amorphous phase of the specimen. Of note, the ^{1}H NMR spectrum complements FT-IR analysis of ɣ-PGA NPs. The chemical shift in ppm at 1.96–2.3, 2.24, 3.55–3.80, and 8.37 ppm represents protons of β-CH2, ɣ-CH2, α-CH2, and amide, respectively.

Notably, the obtained results confirmed the consistency of a pure case of potassium poly gamma glutamate. Moreover, morphological studies using TEM images showed the formation of an oval shape with small particle size ɣ-PGA NPs with sizes of 31.75–32.69 nm, 18.63–21.66 nm, and 37.57–39.22 nm for B4, B5, and B6, respectively. ɣ-PGA NPs were biosynthesized purely using the three new bacterial isolates. Furthermore, ɣ-PGA NPs showed no hemolysis results, i.e., negligible hemolysis was detected even at high concentrations of ɣ-PGA NPs (512 μg/mL).

Using PBMC to detect ɣ-PGA NPs cytotoxicity against the immune system, there was no effect on cell viability. The report of the present study conclusively is to biosynthesize eco-friendly NPs with small particle sizes in order to be used in many biomedical applications safely.

Author Contributions: E.M.E.: Conceptualization, Methodology, Data Curation, Writing. A.M.M.: Supervision, Resources, Writing—Review and Editing. A.A.F.: Supervision, Characterization, Writing—Review and Editing. M.I.Z.: Supervision, Writing—Review and Editing. M.A.-F.: Supervision, Resources, Writing—Review and Editing. D.H.M.A.: Resources. W.N.H.: Resources. All authors have read and agreed to the published version of the manuscript.

Institutional Review Board Statement: This study was conducted in accordance with the Declaration of Helsinki and approved by the Institutional Review Board of Beni-Suef University, Egypt (BNS/2021/10).

Informed Consent Statement: Informed consent was obtained from all subjects involved in the study.

Data Availability Statement: All data can be found in the article.

Conflicts of Interest: The authors declare no conflict of interests.

References

1. Doppalapudi, S.; Jain, A.; Khan, W.; Domb, A.J. Biodegradable polymers—An overview. *Polym. Adv. Technol.* **2014**, *25*, 427–435. [CrossRef]
2. Shih, I.L.; Van, Y.T.; Yeh, L.C.; Lin, H.G.; Chang, Y.N. Production of a biopolymer flocculant from *Bacillus licheniformis* and its flocculation properties. *Bioresour. Technol.* **2001**, *78*, 267–272. [CrossRef] [PubMed]
3. Buescher, J.M.; Margaritis, A. Microbial biosynthesis of polyglutamic acid biopolymer and applications in the biopharmaceutical, biomedical and food industries. *Crit. Rev. Biotechnol.* **2007**, *27*, 1–19. [CrossRef] [PubMed]
4. Ogunleye, A.; Bhat, A.; Irorere, U.V.; Hill, D.; Williams, C.; Radecka, I. Poly-ɣ-glutamic acid: Production, properties and applications. *Microbiology* **2015**, *161*, 1–17. [CrossRef]
5. Cao, M.; Geng, W.; Liu, L.; Song, C.; Xie, H.; Guo, W.; Jin, Y.; Wang, S. Glutamic acid independent production of poly-ɣ-glutamic acid by *Bacillus amyloliquefaciens* LL3 and cloning of pgs BCA genes. *Bioresour. Technol.* **2010**, *201*, 4251–4257.
6. Akagi, T.; Baba, M.; Akashi, M. Preparation of nanoparticles by the self-organization of polymers consisting of hydrophobic and hydrophilic segments: Potential applications. *Polymer* **2007**, *48*, 6729–6747. [CrossRef]
7. Bodnár, M.; Kjøniksen, A.; Molnár, R.; Hartmann, J.; Daróczi, L.; Nyström, B.; Borbély, B. Nanoparticles formed by complexation of poly-gamma-glutamic acid with lead ions. *J. Hazard. Mater.* **2008**, *153*, 1185–1192. [CrossRef]
8. Candela, T.; Fouet, A. Poly-gamma-glutamate in bacteria. *Mol. Microbiol.* **2006**, *60*, 1091–1098. [CrossRef]
9. Ko, Y.H.; Gross, R.A. Effects of glucose and glycerol on ɣ-poly(glutamic acid) formation by *Bacillus licheniformis* ATCC 9945a. *Biotechnol. Bioeng.* **1998**, *57*, 430–437. [CrossRef]

10. Ashiuchi, M.; Kamei, T.; Baek, D.-H.; Shin, S.-Y.; Sung, M.-H.; Soda, K.; Yagi, T.; Misono, H. Isolation of *Bacillus subtilis* (chungkookjang), a poly-ɣ-glutamate producer with high genetic competence. *Appl. Microbiol. Biotechnol.* **2001**, *57*, 764–769. [CrossRef]

11. Shih, I.L.; Van, Y.T. The production of poly-(ɣ-glutamic acid) from microorganisms and its various applications. *Bioresour. Technol.* **2001**, *79*, 207–225. [CrossRef] [PubMed]

12. Park, C.; Choi, J.; Choi, Y.; Nakamura, H.; Shimanouchi, K.; Horiuchi, T.; Misono, H.V.T.; Soda, K.; Ashiuchi, M.; Sunga, M. Synthesis of super-high-molecular-weight poly-ɣ-glutamic acid by *Bacillus subtilis* subsp. Chungkookjang. *J. Mol. Catal. B Enzym.* **2005**, *35*, 128–133. [CrossRef]

13. Kang, H.S.; Park, S.-H.; Lee, Y.-G.; Son, T.-I. Polyelectrolyte Complex Hydrogel Composed of Chitosan and Poly(g-Glutamic Acid) for Biological Application: Preparation, Physical Properties, and Cytocompatibility. *J. Appl. Polym. Sci.* **2010**, *116*, 2658–2667. [CrossRef]

14. Hsieh, C.Y.; Tsai, S.P.; Wang, D.M.; Chang, Y.N.; Hsieh, H.J. Preparation of ɣ-PGA/chitosan composite tissue engineering matrices. *Biomaterials* **2005**, *26*, 5617–5623. [CrossRef]

15. Lin, Y.H.; Chung, C.K.; Chen, C.T.; Liang, H.F.; Chen, S.C.; Sung, H.W. Preparation and Characterization of Nanoparticles Shelled with Chitosan for Oral Insulin Delivery. *Biomacromolecules* **2007**, *8*, 146–152. [CrossRef] [PubMed]

16. Ahmed, M.K.; Zayed, M.A.; El-dek, S.I.; Hady, M.A.; El Sherbiny, D.H.; Uskoković, V. Nanofibrous ε-polycaprolactone scaffolds containing Ag-doped magnetite nanoparticles: Physicochemical characterization and biological testing for wound dressing applications in vitro and in vivo. *Bioact. Mater.* **2021**, *6*, 2070–2088. [CrossRef]

17. Mosquera, J.; García, I.; Liz-Marzán, L.M. Cellular Uptake of Nanoparticles versus Small Molecules: A Matter of Size. *Acc. Chem. Res.* **2018**, *51*, 2305–2313. [CrossRef] [PubMed]

18. Khan, I.; Saeed, K.; Khan, I. Nanoparticles: Properties, applications and toxicities. *Arab. J. Chem.* **2019**, *12*, 908–931. [CrossRef]

19. Deenadayalan, A.; Maddineni, P.; Raja, A. Comparison of whole blood and PBMC assays for T-cell functional analysis. *BMC Res. Notes* **2013**, *6*, 120. [CrossRef] [PubMed]

20. Choi, Y.-H.; Yan, G.-H.; Chai, O.H.; Song, C.H. Inhibitory effects of curcumin on passive cutaneous anaphylactoid response and compound 48/80-induced mast cell activation. *Anat. Cell Biol.* **2010**, *43*, 36. [CrossRef]

21. Xu, G.; Zha, J.; Cheng, H.; Ibrahim, M.H.; Yang, F.; Dalton, H.; Cao, R.; Zhu, Y.; Fang, J.; Chi, K.; et al. Engineering Corynebacterium glutamicum for the de novo biosynthesis of tailored poly-ɣ-glutamic acid. *Metab. Eng.* **2019**, *56*, 39–49. [CrossRef]

22. Wei, X.; Tian, G.; Ji, Z.; Chen, S. A new strategy for enhancement of poly-ɣ-glutamic acid production by multiple physicochemical stresses in *Bacillus licheniformis*. *J. Chem. Technol. Biotechnol.* **2015**, *90*, 709–713. [CrossRef]

23. Qiu, Y.; Zhang, Y.; Zhu, Y.; Sha, Y.; Xu, Z.; Feng, X.; Li, S.; Xu, H. Improving poly-(ɣ-glutamic acid) production from a glutamic acid-independent strain from inulin substrate by consolidated bioprocessing. *Bioprocess Biosyst. Eng.* **2019**, *42*, 1711–1720. [CrossRef]

24. El-Sayed, E.M.; Salah, T.A.; Husseiny, S.M. Biosynthesized silver nanoparticles from new bacterial isolate and studying their effect on dermatophyte fungi. *J. Sci. Res. Sci.* **2017**, *34*, 123–141.

25. Pisani, S.; Dorati, R.; Scocozza, F.; Mariotti, C.; Chiesa, E.; Bruni, G.; Genta, I.; Auricchio, F.; Conti, M.; Conti, B. Preliminary investigation on a new natural based poly(gamma-glutamic acid)/Chitosan bioink. *J. Biomed. Mater. Res. Part B Appl. Biomater.* **2020**, *108*, 2718–2732. [CrossRef] [PubMed]

26. Lv, H.; Cui, S.; Yang, Q.; Song, X.; Wang, D.; Hu, J.; Zhou, Y.; Liu, Y. AgNPs-incorporated nanofiber mats: Relationship between AgNPs size/content, silver release, cytotoxicity, and antibacterial activity. *Mater. Sci. Eng. C* **2021**, *118*, 111331. [CrossRef] [PubMed]

27. Jett, B.D.; Hatter, K.L.; Huycke, M.M.; Gilmore, M.S. Simplified agar plate method for quantifying viable bacteria. *BioTechniques* **1997**, *23*, 648–650. [CrossRef]

28. Goto, A.; Kunioka, M. Biosynthesis and Hydrolysis of Poly (ɣ-glutamic acid) from *Bacillus subtilis* IF03335. *Biosci. Biotechnol. Biochem.* **2014**, *56*, 1031–1035. [CrossRef]

29. Jeevan, P.; Ramya, K.; Rena, A.E. Extracellular biosynthesis of silver nanoparticles by culture supernatant of *Pseudomonas aeruginosa*. *Indian J. Biotechnol.* **2012**, *11*, 72–76.

30. Singh, V.; Chaudhary, D.; Mani, I. Molecular characterization and modeling of secondary structure of 16S rRNA from *Aeromonas veronii*. *Int. J. Appl. Biol. Pharm. Technol.* **2012**, *3*, 253–260.

31. Prasad, P.; Turner, M.S. What bacteria are living in my food? An open-ended practical series involving identification of unknown foodborne bacteria using molecular techniques. *Biochem. Mol. Biol. Educ.* **2011**, *39*, 384–390. [CrossRef] [PubMed]

32. Tripathi, P.; Banerjee, G.; Gupta, M.K.; Saxena, S.; Ramteke, P.W. Assessment of phylogenetic affiliation using 16S rRNA gene sequence analysis for *Pseudomonas aeruginosa* in patients of lower respiratory tract infection. *Indian J. Med. Res.* **2013**, *138*, 557–559. [PubMed]

33. Chen, Y.; Yan, X.; Zhao, J.; Feng, H.; Li, P.; Tong, Z.; Yang, Z.; Li, S.; Yang, J.; Jin, S. Preparation of the chitosan/poly(glutamic acid)/alginate polyelectrolyte complexing hydrogel and study on its drug releasing property. *J. Carbohydr. Polym.* **2018**, *191*, 8–16. [CrossRef]

34. Khalil, I.R.; Irorere, V.U.; Radecka, I.; Burns, A.T.; Kowalczuk, M.; Mason, J.L.; Khechara, M.P. Poly-ɣ-glutamic acid: Biodegradable polymer for potential protection of beneficial viruses. *Materials* **2016**, *9*, 28. [CrossRef] [PubMed]

35. Khan, M.; Naqvi, H.N.; Ahmad, M. Comparative study of the cytotoxic and genotoxic potentials of zinc oxide and titanium dioxide nanoparticles. *Toxicol. Rep.* **2015**, *2*, 765–774. [CrossRef] [PubMed]

36. Martínez-Rodríguez, N.L.; Tavárez, S.; González-Sánchez, Z.I. In vitro toxicity assessment of zinc and nickel ferrite nanoparticles in human erythrocytes and peripheral blood mononuclear cell. *Toxicol. Vitr.* **2019**, *57*, 54–61. [CrossRef] [PubMed]

37. Jiang, L.; Yu, Y.; Li, Y.; Yu, Y.; Duan, J.; Zou, Y.; Li, Q.; Sun, Z. Oxidative Damage and Energy Metabolism Disorder Contribute to the Hemolytic Effect of Amorphous Silica Nanoparticles. *Nanoscale Res. Lett.* **2016**, *11*, 57. [CrossRef]

38. Aimola, I.A.; Inuwa, H.M.; Nok, A.J.; Mamman, A.I.; Habila, N.; Muhammad, A.; Ndidi, U.S.; Ignatius, B.; Jande, P.L.; Isaac, L.C.; et al. Isolation of peripheral blood mononuclear cells using glycerol density gradient. *Cell Biochem. Biophys.* **2014**, *68*, 583–585. [CrossRef]

39. Hamburger, A.W.; Dunn, F.E.; Tencer, K.L. Isolation of peripheral blood mononuclear cells using glycerol density gradient, Separation on percoll density gradients of cells derived from malignant ascites of mice. *JNCI J. Natl. Cancer Inst.* **1983**, *70*, 157–160. [CrossRef]

40. Rushdy, A; Gomaa, E. Antimicrobial compounds produced by probiotic *Lactobacillus brevis* isolated from dairy products. *Ann. Microbiol.* **2013**, *63*, 81–90. [CrossRef]

41. Yu, N.A.B.; Mirgorod, A.; Fedosyuk, V.M. Physico-Chemical Properties of Nanoparticles Functionalized by Polypyrrole. *J. Nano-Electron. Phys.* **2013**, *5*, 5–7.

42. Panda, P.K.; Yang, J.M.; Chang, Y.H. Preparation and characterization of ferulic acid-modified water soluble chitosan and poly (ɤ-glutamic acid) polyelectrolyte films through layer-by-layer assembly towards protein adsorption. *Int. J. Biol. Macromol.* **2021**, *171*, 457–464. [CrossRef] [PubMed]

43. Lee, H.Y.; Jeong, Y.I.; Choi, K.C. Hair dye-incorporated poly-ɤ-glutamic acid/glycol chitosan nanoparticles based on ion-complex formation. *Int. J. Nanomed.* **2011**, *6*, 2879–2888. [CrossRef]

44. Liu, C.; Peng, Y.; Zhou, F.; Yin, Y.; Huang, X.; Wang, L.; Wang, W.; Zhou, W.; Tang, D. Large-scale synthesis and quantitative characterization of size-controllable potassium tungsten bronze nanowires. *J. Phys. D. Appl. Phys.* **2018**, *51*, 095305. [CrossRef]

45. Kar, M.; Pauline, M.; Sharma, K.; Kumaraswamy, G.; Sen Gupta, S. Synthesis of poly-l-glutamic acid grafted silica nanoparticles and their assembly into macroporous structures. *Langmuir* **2011**, *27*, 12124–12133. [CrossRef]

46. Pereira, C.L.; Antunes, J.C.; Gonçalves, R.M.; Ferreira-Da-Silva, F.; Barbosa, M.A. Biosynthesis of poly-ɤ-glutamic acid and its application in the development of chitosan/poly-ɤ-glutamic acid nanoparticles for drug delivery. *J. Mater. Sci. Mater. Med.* **2012**, *23*, 1583–1591. [CrossRef]

47. Hajdu, I.; Bodnár, M.; Filipcsei, G.; Hartmann, J.F.; Daróczi, L.; Zrínyi, M.; Borbély, J. Nanoparticles prepared by self-assembly of Chitosan and poly-ɤ-glutamic acid. *Colloid Polym. Sci.* **2008**, *286*, 343–350. [CrossRef]

48. Nguyen, Q.T.; Kwak, C.; Lee, W.S.; Kim, J.; Jeong, J.; Sung, M.H.; Yang, J.; Poo, H. Poly-ɤ-glutamic acid complexed with alum induces cross-protective immunity of pandemic H1N1 vaccine. *Front. Immunol.* **2019**, *10*, 1604. [CrossRef]

49. Anju, A.J.; Binod, P.; Pandey, A. Production and characterization of microbial poly-ɤ-glutamic acid from renewable resources. *Indian J. Exp. Biol.* **2017**, *55*, 405–410.

50. Aseichev, A.V.; Azizova, O.A.; Beckman, E.M.; Skotnikova, O.I.; Dudnik, L.B.; Shcheglovitova, O.N.; Sergienko, V.I. Effects of gold nanoparticles on erythrocyte hemolysis. *Bull. Exp. Biol. Med.* **2014**, *156*, 495–498. [CrossRef]

51. Paula, A.J.; Martinez, D.S.T.; Júnior, R.T.A.; Filho, A.G.S.; Alves, O.L.A. Suppression of the hemolytic effect of mesoporous silica nanoparticles after protein corona interaction: Independence of the surface microchemical environment. *J. Braz. Chem. Soc.* **2012**, *23*, 1807–1814. [CrossRef]

52. Lu, B.; Lu, F.; Ran, L.; Yu, K.; Xiao, Y.; Li, Z.; Dai, F.; Wu, D.; Lan, G. Imidazole-molecule-capped chitosan–gold nanocomposites with enhanced antimicrobial activity for treating biofilm-related infections. *J. Colloid Interface Sci.* **2018**, *531*, 269–281. [CrossRef] [PubMed]

53. Reddy, K.M.; Feris, K.; Bell, J.; Wingett, D.G.; Hanley, C.; Punnoose, A. Selective toxicity of zinc oxide nanoparticles to prokaryotic and eukaryotic systems. *Appl. Phys. Lett.* **2007**, *90*, 10–13. [CrossRef] [PubMed]

54. Hanley, C.; Layne, J.; Punnoose, A.; Reddy, K.; Coombs, I.; Coombs, A.; Feris, K.; Wingett, D. Preferential killing of cancer cells and activated human T cells using ZnO nanoparticles. *Nanotechnology* **2008**, *19*, 295103. [CrossRef]

55. Tsai, W.B.; Lai, H.Y.; Lee, J.L.; Lo, C.W.; Chen, W.S. Enhancement of the cytotoxicity and selectivity of doxorubicin to hepatoma cells by synergistic combination of galactose-decorated ɤ-poly(glutamic acid) nanoparticles and low-intensity ultrasound. *Langmuir* **2014**, *30*, 5510–5517. [CrossRef] [PubMed]